



Investigating the effects of growth rate and temperature on the B/Ca ratio and $\delta^{11}\text{B}$ during inorganic calcite formation



Karina Kaczmarek ^{a,*}, Gernot Nehrke ^a, Sambuddha Misra ^b, Jelle Bijma ^a, Henry Elderfield ^b

^a Alfred-Wegener-Institut Helmholtz-Zentrum für Polar- und Meeresforschung, Am Handelshafen 12, 27570 Bremerhaven, Germany

^b Department of Earth Science, University of Cambridge, Downing Site, CB2 3EQ Cambridge, UK

ARTICLE INFO

Article history:

Received 23 July 2015

Received in revised form 23 November 2015

Accepted 10 December 2015

Available online 12 December 2015

Keywords:

Calcite

Boron isotopes

B/Ca

Fractionation

Temperature

Growth rate

Inorganic precipitation

ABSTRACT

To deconvolve the effect of growth rate and temperature on the boron partitioning into calcite and its isotope fractionation, seeded calcite precipitation experiments were performed at a constant temperature and various growth rates and at a constant growth rate and various temperatures. We show that boron partitioning increases with increasing growth rate and decreases with increasing temperature. The B isotope fractionation between calcite and $\text{B}(\text{OH})_4^-$ increases with increasing growth rate favoring the lighter B isotope for incorporation into calcite whereas no effect of temperature was observed within the temperature range investigated (12 °C to 32 °C). At the lowest temperature and growth rate $\delta^{11}\text{B}$ of the calcite almost equals that of $\text{B}(\text{OH})_4^-$ in solution. Applying the surface entrapment model (SEMO) of Watson and Liang (1995) to our data, we demonstrate that the observed effects of temperature and growth rate on B concentration can be explained by processes in the near surface layer of the calcite crystal.

© 2015 The Authors. Published by Elsevier B.V. This is an open access article under the CC BY-NC-ND license (<http://creativecommons.org/licenses/by-nc-nd/4.0/>).

1. Introduction

Element ratios and isotope signatures trapped within the crystal lattice of marine biogenic calcite are strongly influenced by the physio-chemical conditions of their growth environment and can thus be utilized as paleo-oceanographic/paleo-climate proxies (e.g. Urey, 1947; Boyle, 1988; Wefer et al., 1999). The incorporation of boron (B) into coral and foraminiferal calcium carbonate (CaCO_3) is of particular interest since its concentration and isotopic composition is assumed to record information about the carbonate system at the time of calcification (Yu and Elderfield, 2007; Sanyal et al., 2000, 2001). In aqueous solution B speciates between trigonal boric acid ($\text{B}(\text{OH})_3$) and tetrahedral borate ($\text{B}(\text{OH})_4^-$) whose concentration and isotopic composition are strongly pH dependent (DOE, 1994; Hemming and Hanson, 1992). Pioneering work of Hemming and Hanson (1992) followed by numerous field and culture studies on foraminifers and corals (e.g. Sanyal et al., 1996, 2001; Hönisch et al., 2004; Reynaud et al., 2004; Foster, 2008; Rae et al., 2011) has established that the isotopic signature of B ($\delta^{11}\text{B}$) of marine carbonates generally tracks the $\delta^{11}\text{B}$ of $\text{B}(\text{OH})_4^-$ suggesting that $\text{B}(\text{OH})_4^-$ is predominantly incorporated into calcium carbonate from ambient seawater with very little isotopic

fractionation. Consequently, the isotope composition of B in calcite should reflect that of $\text{B}(\text{OH})_4^-$ in solution. Recently, Uchikawa et al. (2015) hypothesized that in inorganic calcite there is possibility for a rate dependent incorporation of the isotopically heavy $\text{B}(\text{OH})_3$ at faster growth rates. However, this hypothesis was not directly inferred from B isotope analysis but on calculations based on B concentration data.

Boron isotopic composition of fossilized marine carbonates are an emerging proxy to reconstruct past seawater pH changes (e.g. Sanyal and Bijma, 1999; Hönisch and Hemming, 2005; Foster, 2008; Bartoli et al., 2011; Foster et al., 2012) and the B/Ca ratios of several species of benthic foraminifers have been utilised to assess the saturation state of seawater CO_3^{2-} (Yu and Elderfield, 2007; Yu et al., 2007; Brown et al., 2011; Rae et al., 2011). However, B/Ca and $\delta^{11}\text{B}$ values of foraminiferal calcite from field studies show a significant species specific variability (so called “vital effects”). These vital effects include physiological processes of the foraminifers and their symbionts which lead to shifts in the carbon and boron equilibria in their micro-habitat resulting in deviation from empirical estimates (Hönisch et al., 2003; Kaczmarek et al. 2015). Due to the diversity and the interconnection between parameters affecting the B signature in foraminiferal calcite it is difficult to evaluate the impact of a single parameter such as temperature on the measured signal. This is well illustrated by a comparison of several field studies that draw a divergent picture concerning the temperature effect on the B incorporation in foraminifers (Allen and Hönisch, 2012). Besides temperature other important factors such as growth rate might affect the B incorporation into calcium carbonate.

* Corresponding author at: Am Handelshafen 12, 27570 Bremerhaven, Germany.

E-mail addresses: karina.kaczmarek@awi.de (K. Kaczmarek), gernot.nehrke@awi.de (G. Nehrke), sm929@cam.ac.uk (S. Misra), jelle.bijma@awi.de (J. Bijma), he101@cam.ac.uk (H. Elderfield).

Any chemical process like crystal growth has a temperature dependence (McIntire, 1963). A change in temperature of a system alters the kinetics of chemical processes such as growth rate. From the perspective of inorganic precipitation reactions, the strong temperature dependence of the growth rate may have consequences on the element partitioning and isotope fractionation during crystal growth (e.g. Lorens, 1981; Rimstidt et al., 1998; Tesoriero and Pankow, 1996; Gussone et al., 2005; Gabitov and Watson, 2006; Tang et al., 2008a,b). Based on atomic force microscopy (AFM) investigations on inorganically formed calcite, Ruiz-Agudo et al. (2012) inferred that a slow growth rate may promote a higher B incorporation, however, the impact of growth rate on B isotopes was not investigated in that study. On the contrary, independent experimental results published in recent year (Gabitov et al., 2014; Mavromatis et al., 2015; Uchikawa et al., 2015) consistently show that B incorporation actually increases with growth rate during inorganic calcite precipitation. These pioneering studies did not allow firm conclusions to be drawn about the B isotope fractionation between solution and calcite at different growth rates. More specifically, the Gabitov et al. (2014) investigation of the relationship between growth rate and B isotopes in calcite were inconclusive due to the comparatively large analytical uncertainty (4%, 2σ) in determination of $\delta^{11}\text{B}$ of solids and by the absence on $\delta^{11}\text{B}$ measurements of the solution phase.

The exact mechanism of foraminiferal biomineralization remains poorly understood. Hence, it is not possible to investigate the effects of temperature and growth rate on B/Ca and $\delta^{11}\text{B}$ separately. Fundamental observations from inorganic systems coupled with controlled culture experiments should allow us to develop a better understanding of the impact of temperature and growth rate on biomineralization. Importantly, the temperature dependence of calcite growth rate, as observed during inorganic calcite precipitation experiments, makes it necessary to conduct crystal growth experiments under decoupled temperature and growth rate. This will then allow separating the effects of temperature and growth rate on B co-precipitation and fractionation. In this study we have assessed the role of temperature and growth rate on the B concentration and its isotopic composition in calcite using highly controlled precipitation experiments for: (1) calcite growth across a temperature range of 20 °C (12 to 32 °C) at constant growth rate, and (2) calcite growth at constant temperature (22 °C) and two different growth rates.

2. Material and methods

2.1. Experimental setup

Calcite precipitation was performed in a 250 ml quartz-glass beaker containing 150 ml of a growth solution supersaturated with respect to calcite (see Section 2.2.). In order to trigger precipitation five mg of calcite powder (Aldrich; 50–100 μm sized aggregates containing 5–10 μm sized grains, as characterized by scanning electron microscopy; SEM) were added to the supersaturated solution. In order to transfer the powder into the quartz-glass beaker quickly, 1 ml of the growth solution was pipetted into a 2 ml Eppendorf vial containing the pre-weighed calcite powder. The suspension was then transferred back into the quartz-glass beaker and this step repeated twice to achieve a quantitative transfer. During the precipitation of calcite the concentration of Ca, pH, and the saturation state of calcite (Ω) were kept constant using an automated chemostat system (Fig. 1). This chemostat system consists of a titrator (Titrand 902, Metrohm), three burettes (Dosino 800, Metrohm), a Ca-ion selective electrode (6.1241.050, Metrohm), and a pH electrode (6.0262.100 Ecotrode Plus, Metrohm). The chemostat system was controlled by the software tiamo 2.3 (Metrohm). Burette 1 contained a 0.02 M CaCl_2 , 0.04 M $\text{B}(\text{OH})_3$, and 0.7 M NaCl solution. Burette 2 contained a 0.02 M Na_2CO_3 and a 0.7 M NaCl (all chemicals were obtained from Merck in the quality suprapure®). A drop in the Ca concentration detected by the Ca sensitive electrode triggered

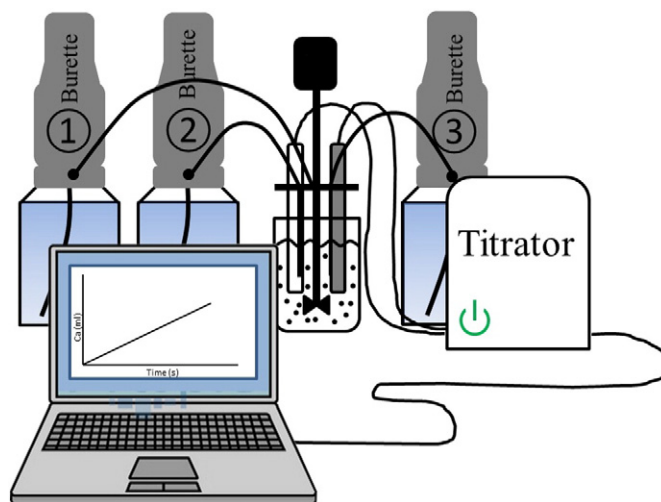


Fig. 1. Illustration of the experimental set-up. Overgrowth of calcite seeds was performed in a beaker containing a growth solution with a Ω of 2.5–4. Ca^{2+} and pH sensors dipped into the growth solutions detected the loss of [Ca], [B], and the increase of $[\text{H}^+]$ triggering 3 burettes to keep the chemical composition constant.

burette 1 and 2 to add simultaneously the same volume into the growth solution until the final Ca concentration was reset to initial values. The Ca and the pH electrodes were logged during precipitation every 60 s and the temperature every 120 s. The CO_2 produced during the precipitation of calcite reduces the pH of the solution and subsequently lowers the Ω . To maintain constant Ω , pH and dissolved inorganic carbon (DIC) concentration during calcite precipitation, the pH electrode was employed to trigger the third burette containing a 0.01 M $\text{HCO}_3^-/\text{CO}_3^{2-}$ (in a ratio identical to the growth solution) and a 0.7 M NaCl solution. The calcite powders were kept in suspension throughout the experiments by stirring the solution (200 rpm) by an agitator (model BDC250, Caframo) equipped with a Teflon coated axial impeller (Bohlander C378-12). The precipitation experiments were terminated when 55 ml of burettes 1 and 2 had been added, respectively. This ensured (1) sufficient overgrowth of calcite (~15 times the mass of the initial seeds) (2) the B concentration in the overgrowth met the analytical requirements. Subsequently, the growth solution was vacuum filtered using a 0.2 μm PC filter (Whatman 110606). In order to achieve a quantitative recovery of calcite crystals and to remove adsorbed B from the crystal surface the beaker was rinsed three times with 30 ml of a calcite saturated solution (prepared from suprapure calcite powder and 18.2 M-Ohm di-ionized water). In a second step 90 ml of di-ionized water (resistance = 18.2 M-Ohm) was used to remove the residual Ca from previous step. Pilot experiments performed with a known mass of powder showed that these washing steps did not lead to a detectable loss of material or addition of B. The calcite crystals were dried in an oven at 50 °C for 12 h, and weighed using an analytical balance (Mettler Toledo, XP Excellence Plus) with a resolution of 0.1 μg . For B analysis (see Section 2.4) all calcite powder recovered from the experiment was dissolved in 0.5 M HNO_3 (Merck, Suprapure® quality). All experiments were performed in a temperature-controlled laboratory.

2.2. Precipitation experiments

Precipitation experiments were performed at 12, 22, and 32 °C. Since temperature has a strong effect on the precipitation rate, it was necessary to modify the solution compositions for the temperature experiments to achieve comparable growth rates independent of temperature. Solution compositions giving comparable growth rates have been determined by means of pilot experiments. The key objective of these pre-experiments was to find a precipitation rate that was (1) not too

fast (not diffusion limited), (2) experimentally feasible (allowing accurate control by the chemostat system without the need to re-calibrate electrodes), and (3) resulted in a significant amount of precipitate – a necessary requirement for robust $\delta^{11}\text{B}$ analysis. The first step in the process was to calculate the chemistry of the growth solutions using the chemical speciation code V. MINTEQ 3.0 (Gustafsson, 2008). Based on the pilot experiments, a supersaturation ($\Omega = \text{IAP } K_{\text{sp}}^{-1}$) of ~ 4 with respect to calcite was optimal for the present set of experiments. Since it had been shown that the Ca/CO₃ stoichiometry in solution strongly influences the growth rate of calcite (e.g. Nehrke et al., 2007; Wolthers et al., 2012), we achieved different growth rates (R) by adapting the Ca concentration in the different growth solutions. The growth rate is defined as:

$$R = (mt_1 - mt_0)/mt_0/t \quad (1)$$

where mt_0 is the initial mass of the calcite seed at the beginning of the experiment, mt_1 the mass of the total calcite at the end, and t the duration of the experiment. The determination of absolute growth rates that allow for a direct comparison between different experimental setups and seed materials is difficult to achieve. In an ideal scenario the growth rate would be reported in units of m s^{-1} . However, in most cases it is not possible to experimentally determine the growth rate directly in units of m s^{-1} without making multiple assumptions. A re-calculation from different units, like precipitated mass/amount of material per surface area and time, requires an exact knowledge on how the crystal geometry and surface area change during crystal precipitates. The surface area of the precipitate can be measured by BET (a method by which the surface area of a solid is determined by the adsorption of gas molecules) for the seed material and the precipitate at the end of the experiment if enough material is available. Often the size of the crystals and their surface area and topography is estimated based on SEM micrographs. Especially, in the case of seed material that is present in the form of complex aggregates (often the case for calcite powders) this method is associated with a very large error since the growth of these aggregates is very complex (data on surface roughness and reactive sites like kinks and steps are hard to estimate). To avoid unreliable/qualitative assumptions in the determination of growth rates, we report growth rates normalized to the weight of the seeds present in the beginning of the experiment. This will allow us to compare results from different experiments in a direct and standardized way.

Our pilot study showed that it was possible to conduct precipitation experiments with the similar growth rates at 22 and 32 °C. In order to minimize the impact of pH on the B speciation and isotopic composition of the respective species, the pH of all growth solutions was held constant (~ 8.7). A 0.7 M NaCl solution was used as the precipitation matrix to obtain an ionic strength (I) similar to that of seawater. The B concentration was set at 0.0035 M, ~ 10 times higher than natural seawater. The elevated B concentration does not alter the B speciation since Su and Suarez (1995) showed that polynuclear B species starts to form only at concentrations $\geq 25 \text{ mmol L}^{-1}$.

All chemicals used for the experiments were obtained from Merck (Suprapure® quality) and dissolved in de-ionized water (18.2 M-Ohm). All precipitation experiments were repeated in quadruplicate. Species distribution and Ω of the growth solutions were calculated using the chemical speciation code VisualMINTEQ 3.0 (Gustafsson, 2008) based on measured input parameters ([Ca], [B], [DIC], pH) and weighted NaCl. VisualMINTEQ calculates species distribution using the Debye–Hückel equation. For C the pK_1 and pK_2 determined by Plummer and Busenberg (1982) were used and boric acid was added into the database of VisualMINTEQ 3.0. We chose to work with the pK_B determined by Owen and King (1943) since this value (8.8316, 25 °C) is most suitable for Na–Cl solutions having a M_{NaCl} of 0.725 which is very close to the conditions of our growth solutions ($M_{\text{NaCl}} = 0.7$). Furthermore, the study of Owen and King (1943)

provides a temperature correction for pK_B . The pK_B values used in this study for 12, 22, and 32 °C are 8.951, 8.859, and 8.778.

2.3. Analysis of the solutions

Before and after each experiment salinity of the growth solution was measured and aliquots were sampled for determination of [Ca], [B], $\delta^{11}\text{B}$, and [DIC]. Salinity measurements were performed using a conductivity meter (WTW Multi 340i) interfaced with a TetraCon 325 conductivity sensor. Calcium concentration was determined by a Thermo Elemental (TJA) IRIS Intrepid ICP-OES Spectrometer using a Merck 4 multi element standard. The average internal error, as estimated by multiple measurements of the reference material, was $\pm 3.5\%$. Determination of [DIC] was performed photometrically in triplicates with a TRAACS CS800 QuaAatro autoanalyzer with an average reproducibility of $\pm 10 \mu\text{mol/l}$ based on measurements of an in-house standard (North Sea Seawater) that is calibrated against certified reference material batch No. 54 of Dickson (Scripps Institution of Oceanography). Before each run the pH electrode was calibrated using NIST/DIN buffers (pH 6.865 and 9.180) giving at least a R^2 of 98%.

2.4. Boron analysis

Boron isotopes were analysed by Thermo® Neptune Plus®, a multi collector, sector field, high-resolution inductively coupled plasma mass spectrometer, following the method described in Misra et al. (2014a, 2014b). Boron isotopic compositions are reported as per mil (‰) deviation from NIST SRM 951a ($^{11}\text{B}/^{10}\text{B} = 4.04362 \pm 0.00137$) (Catanzaro et al., 1970) where:

$$\delta^{11}\text{B}(\text{‰}) = \left(\left[\frac{^{11}\text{B}/^{10}\text{B}_{\text{sample}}}{^{11}\text{B}/^{10}\text{B}_{\text{NIST-951a}}} \right] - 1 \right) \times 1000 \quad (2)$$

Boron isotope analyses were done following Sample–Standard Bracketing (SSB) technique. Samples were concentration matched, typically at $\pm 5\%$, with the standard and were analysed in triplicate. All samples and standards were analysed in 0.3 M HF matrix to facilitate rapid boron wash out (Misra et al., 2014a, 2014b). An ESI® PFA microflow self-aspirating nebulizers with sample uptake rate of 20 $\mu\text{l}/\text{min}$ was used for sample aspiration. We used Saville® PTFE® scott type, single pass, spray chamber and ESI® platinum injector as HF resistant sample introduction system. High performance nickel extraction cones (Jet sampler and 'X' skimmer) were used to achieve maximum B sensitivity. The Neptune® was operated in low-resolution mode ($M/\Delta M = 450$) and at 1350 W RF power. The ^{10}B and ^{11}B ion beams were collected in L3 ($10^{-12} \Omega$ resistor) and H3 ($10^{-11} \Omega$ resistor) Faraday cups, respectively. Instrumental operational conditions were optimised daily and a threshold sensitivity of $>0.5 \text{ V}$ on ^{11}B for a 40 ppb B solution was set as target. A long (600 s) baseline determination was performed at the beginning of each instrument session. Each sample analysis, with 25 cycles of 8.3 s integration time, lasted ~ 4 min and required $\sim 3.5 \text{ ng}$ of B. The average internal precision for triplicate analyses of samples (2σ , $n = 3$), calculated for 72 samples analysed over 4 instrument sessions, was 0.24‰. Three standards of known isotopic composition (NIST 915a, AE 120, and AE 121) were analysed during each instrument session. Our results for NIST 915a ($0.03 \pm 0.32\%$, 2σ , $n = 9$), AE 120 ($-20.32 \pm 0.25\%$, 2σ , $n = 7$), and AE 121 ($19.59 \pm 0.18\%$, 2σ , $n = 7$) are identical to published values (Vogl and Rosner, 2012; Foster et al., 2010). Moreover, $\delta^{11}\text{B}$ values of AE 121 micro-distilled (25 ng-B / sample) from high concentration calcium solution (500 ppm Ca) ($-20.33 \pm 0.21\%$, 2σ , $n = 8$) and in pure form ($-20.16 \pm 0.26\%$, 2σ , $n = 8$) were identical to published values. Prior to mass spectrometric analysis B was separated from the sample matrix by a single-step micro-distillation method, modified after

Gaillardet et al. (2001) and Wang et al. (2010) as described in Misra et al. (2014a, 2014b). Savillex® Teflon® fin legged 5 ml beakers with conical interior were used as the distillation reservoir. Samples were loaded on to the cap of a pre-cleaned beaker – the beaker was tightly closed to avoid B loss – set on a hotplate at 95 °C with the conical end pointing up. The distillation process was carried out for 15 to 18 h to achieve a quantitative distillation of B from the load into the distillate. Sample load volume was kept below 50 µl to avoid the accumulated droplet at the conical end from dropping back onto the cap. Post distillation, beakers were taken off the hotplate, allowed to cool for ~15 min, then 0.5 ml of 0.3 M HF was added and the beakers were capped with pre-cleaned caps. The sample residue left on the cap was taken up in 0.1 M HNO₃ for trace element analysis of the precipitated calcite and for determination of the distillation yield (Misra et al., 2014b). The average error, as estimated by multiple measurements of the reference materials, was ±4%.

3. Results

3.1. Chemical composition of the growth solution

Table 1 shows the measured and calculated chemical parameters of the growth solutions of all experiments. During the course of each precipitation experiment the B concentration in the growth solution decreased by ~30%. Mass balance calculations confirm that this B dilution was caused by the addition of the B free DIC solutions by the titration system (burette 2 and 3) rather than caused by co-precipitation of B into calcite. Since all experiments were terminated after the same amount of titrants was added, an identical depletion is observed. The interpretation of our results is therefore not impaired by this systematic decrease in the solution's B concentration.

The B isotopic composition of growth solutions from before and after each run did not change within the analytical uncertainty (Table 1). On average the δ¹¹B of all growth solutions is −14.11 ± 0.27‰ (2SD). Calcium concentration, pH, DIC, and salinity were kept constant through the course of each experiment/run (Table 1). Fig. 2 shows an example of the logged signal of the Ca sensitive electrode (A) and the corresponding addition of CaCl₂ (burette 1) into the growth solution and the signal of the pH electrode (B) with the addition of Na₂CO₃ (burette 2) during one run. The linearity of the chemical evolution of the solution through addition signifies a constant calcite growth rate.

3.2. Boron concentration and isotopic composition of precipitated calcite

3.2.1. Boron concentration

Our data show a distinct growth rate and temperature dependence of the B incorporation into calcite (Table 2). The incorporation of foreign elements into a solid are often expressed in terms of a distribution coefficient (K_D). For the incorporation of a divalent cation such as Mg that substitutes for a Ca ion the K_D is written as Mg/Ca(solid) / Mg/Ca(fluid). In the case of B incorporation the definition of K_D is complicated due to following reasons: (1) Boron undergoes pH dependent speciation, (2) only the charged B(OH)₄[−] species is thought to be incorporated into the crystal lattice, (3) several definitions are discussed in the published literature (e.g. Hemming et al., 1995; Gabitov et al., 2014; Mavromatis et al., 2015; Uchikawa et al., 2015). Since it is still not certain which carbon species controls the B co-precipitation into calcite (e.g. Hemming et al., 1995; Uchikawa et al., 2015), the definition of K_D may lead to different results. Therefore, we compared the results obtained for the following definitions of K_D. Hemming et al. (1995) defined the partition coefficient of B as:

$$K_{D(H1995)} = \frac{HBO_3/CO_3CaCO_3}{[B(OH)_4^-]/[HCO_3^-]_{fluid}} \quad (3)$$

Table 1
Composition of the growth solutions: bp = before precipitation, ap = after precipitation, S = salinity. Information about uncertainties see main text Sections 2.3 and 2.4.

	[Ca] bp (mmol/l)	[Ca] ap (mmol/l)	[B] bp (mmol/l)	[B] ap (mmol/l)	[DIC] bp (mmol/l)	[DIC] ap (mmol/l)	pH	S bp	S ap	δ ¹¹ B bp (‰)	2SD δ ¹¹ B bp (‰)	δ ¹¹ B ap (‰)	2SD δ ¹¹ B ap (‰)	[B(OH) ₄ [−]] (mmol/l)	[CO ₃ ^{2−}] (mmol/l)	[HCO ₃ [−]] (mmol/l)	Ω	R mg/mg/h
12 °C																		
	R = 0.18 mg mg ^{−1} h ^{−1}																	
RUN 1	1.18	1.21	3.65	2.44	6.33	6.08	8.60	43	42	−14.24	0.50	−14.01	0.29	1.18	0.15	4.47	2.98	0.17
RUN 2	1.17	1.17	3.70	2.53	6.38	6.19	8.66	43	42	−14.15	0.36	−14.29	0.34	1.31	0.17	4.44	3.33	0.18
RUN 3	1.20	1.23	3.66	2.49	6.37	6.20	8.64	43	43	−14.34	0.18	−14.03	0.24	1.26	0.16	4.47	3.34	0.19
RUN 4	1.17	1.22	3.66	2.46	6.46	6.46	8.63	43	42	−14.31	0.37	−13.98	0.56	1.23	0.16	4.61	3.31	0.17
22 °C																		
	R = 0.69 mg mg ^{−1} h ^{−1}																	
RUN 5	0.72	0.72	3.72	2.55	5.17	5.16	8.76	43	41	−14.09	0.59	−14.27	0.23	1.74	0.22	3.55	2.81	0.54
RUN 6	0.73	0.76	3.67	2.47	5.08	5.08	8.75	43	42	−14.02	0.19	−14.27	0.04	1.69	0.21	3.50	2.83	0.61
RUN 7	0.72	0.75	3.68	2.53	5.29	5.06	8.76	43	42	−14.11	0.18	−14.21	0.24	1.72	0.22	3.56	2.85	0.85
RUN 8	0.72	0.70	3.67	2.54	5.23	4.79	8.75	43	41	−14.10	0.16	−13.99	0.11	1.70	0.21	3.46	2.64	0.75
22 °C																		
	R = 1.44 mg mg ^{−1} h ^{−1}																	
RUN 9	1.07	1.13	3.67	2.55	5.09	5.12	8.77	43	42	−14.01	0.04	−14.13	0.09	1.73	0.21	3.54	4.32	1.50
RUN 10	1.07	1.03	3.65	2.57	5.07	5.31	8.76	43	41	−14.35	0.22	−14.19	0.06	1.72	0.22	3.57	4.11	1.42
RUN 11	1.05	1.02	3.65	2.50	5.08	4.81	8.75	43	42	−14.03	0.07	−13.92	0.19	1.68	0.21	3.41	3.81	1.45
RUN 12	1.06	1.08	3.66	2.56	5.05	4.89	8.75	43	43	−14.03	0.12	−13.91	0.27	1.69	0.21	3.44	3.94	1.40
32 °C																		
	R = 1.5 mg mg ^{−1} h ^{−1}																	
RUN 13	0.70	0.76	3.69	2.49	5.20	5.57	8.73	43	43	−14.04	0.08	−13.97	0.13	1.84	0.27	3.82	3.79	1.61
RUN 14	0.71	0.74	3.76	2.54	5.22	5.97	8.73	43	44	−13.96	0.28	−13.95	0.46	1.88	0.28	3.98	3.94	1.62
RUN 15	0.71	0.76	3.79	2.57	5.17	6.03	8.73	43	44	−14.25	0.07	−14.22	0.07	1.91	0.28	3.97	3.99	1.61
RUN 16	0.70	0.75	3.74	2.56	5.12	5.77	8.72	43	43	−13.97	0.38	−14.23	0.14	1.86	0.27	3.88	3.72	1.59

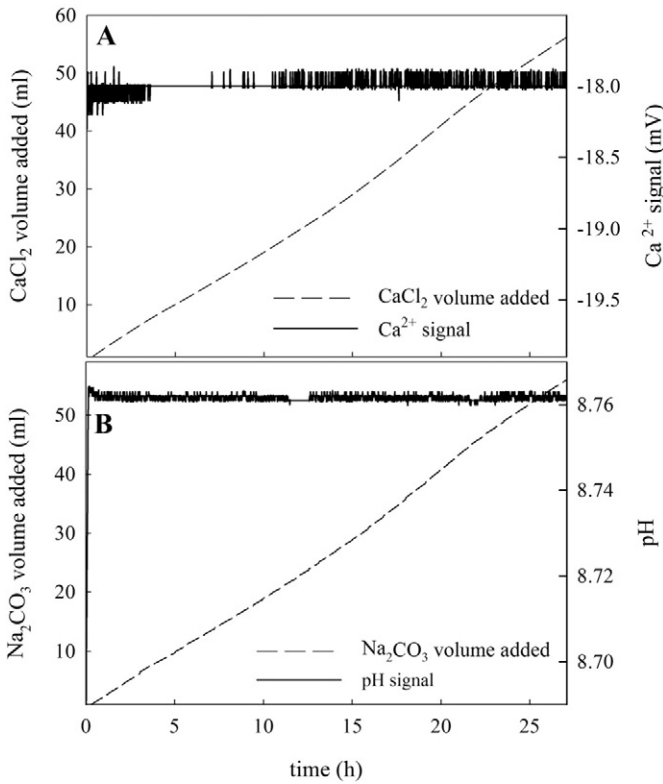


Fig. 2. (A) Ca^{2+} signal (right y-axis) and the corresponding CaCl_2 addition into the growth solution (left y-axis) during the course of one run at 22°C and $R = 0.69 \text{ (mg mg}^{-1} \text{ h}^{-1})$. (B) Corresponding recorded pH (right y-axis) and Na_2CO_3 addition (left y-axis). In both cases a linear trend for the volumetric dosing is observed indicating a constant precipitation rate.

Since HBO_3 and CO_3 species cannot be measured directly but appear in stoichiometric abundance of B and Ca in calcite, Yu and Elderfield (2007) simplified this equation to:

$$K_D = \frac{B/\text{Ca}_{\text{CaCO}_3}}{[\text{B}(\text{OH})_4^-]/[\text{HCO}_3^-]_{\text{fluid}}} \quad (4)$$

Table 2

Measured B data of precipitated calcites ($\delta^{11}\text{B} + [\text{B}]$), calculated $\delta^{11}\text{B}$ of $\text{B}(\text{OH})_4^-$ using (8), B isotope fractionation (ϵ) between calcite and $\text{B}(\text{OH})_4^-$. For details about 2σ uncertainties see Appendix A. The calcite B concentration represents the B concentration in the overgrowth.

	$\delta^{11}\text{B}$ calcite (‰)	2SD (‰)	$\delta^{11}\text{B}$ $\text{B}(\text{OH})_4^-$ (‰)	2 σ (‰)	ϵ (‰)	2 σ (‰)	B calcite (mg/kg)	2SD (mg/kg)	Seeds (mg)	Over growth (mg)
12 °C $R = 0.18 \text{ mg mg}^{-1} \text{ h}^{-1}$										
RUN 1	-27.80	0.51	-28.96	0.76	1.16	0.92	56	2	4.97	73
RUN 2	-27.51	0.17	-28.33	0.71	0.82	0.73	66	3	4.98	80
RUN 3	-27.62	0.18	-28.50	0.67	0.88	0.69	67	3	4.97	79
RUN 4	-27.98	0.09	-28.64	0.57	0.66	0.58	64	3	4.98	78
22 °C $R = 0.69 \text{ mg mg}^{-1} \text{ h}^{-1}$										
RUN 5	-24.53	0.16	-25.05	0.59	0.52	0.61	69	3	4.97	72
RUN 6	-24.52	0.54	-25.13	0.62	0.61	0.82	59	2	4.98	78
RUN 7	-24.42	0.02	-25.07	0.59	0.65	0.59	56	2	4.98	88
RUN 8	-24.41	0.38	-25.06	0.58	0.65	0.70	59	2	4.97	79
22 °C $R = 1.44 \text{ mg mg}^{-1} \text{ h}^{-1}$										
RUN 9	-26.43	0.19	-25.29	0.61	-0.93	0.64	112	4	4.98	77
RUN 10	-26.66	0.14	-25.19	0.59	-1.47	0.61	112	4	4.99	76
RUN 11	-26.69	0.23	-25.00	0.69	-1.69	0.72	117	5	4.99	79
RUN 12	-26.57	0.10	-25.07	0.58	-1.70	0.59	114	5	4.99	74
32 °C $R = 1.5 \text{ mg mg}^{-1} \text{ h}^{-1}$										
RUN 13	-25.32	0.04	-23.83	0.59	-1.48	0.59	56	2	4.97	79
RUN 14	-25.23	0.31	-23.82	0.58	-1.42	0.65	60	2	4.97	74
RUN 15	-25.08	0.10	-23.98	0.58	-1.10	0.59	54	2	4.97	79
RUN 16	-25.16	0.23	-24.06	0.58	-1.10	0.62	55	2	4.96	80

Replacing $[\text{HCO}_3^-]$ with $[\text{CO}_3^{2-}]$ gives:

$$K_D = \frac{B/\text{Ca}_{\text{CaCO}_3}}{[\text{B}(\text{OH})_4^-]/[\text{CO}_3^{2-}]_{\text{fluid}}} \quad (5)$$

Uchikawa et al. (2015) used the following definition:

$$K_D = \frac{B/\text{Ca}_{\text{CaCO}_3}}{[\text{B}]/[\text{HCO}_3^-]_{\text{fluid}}} \quad (6)$$

and Mavromatis et al. (2015):

$$K_D = \frac{B_{\text{CaCO}_3}}{[\text{B}]/[\text{CO}_3^{2-}]_{\text{fluid}}} \quad (7)$$

K_D values calculated for the experiments according to Eqs. (4) to (7) are presented in Fig. 3 and Table 3. Regardless of the definition of the B partition coefficient we observe the same patterns with respect to experiments performed at 22 and 32 °C. The comparison between treatments performed at a constant T but variable growth rates (R) (green and black diamonds in Fig. 3) demonstrates higher K_D values for increased R . Whereas treatments performed at a constant R but variable T (black and orange diamonds in Fig. 3) demonstrates lower K_D values for an increase in T. Error propagation for calculated K_D values is provided in the Appendix A. As pointed out in Section 3.1 the B concentration of all growth solutions was diluted by ~30% by the end of each experiment. Therefore, for the calculation of the K_D values the mean $\text{B}(\text{OH})_4^-$ concentration (Table 1, calculated from the concentrations before and after each experiment) of the growth solution was employed.

3.2.2. Boron isotope composition of calcite

The $\delta^{11}\text{B}$ values of precipitated calcites are listed in Table 2. We observe that at constant growth rate ($\sim 1.5 \text{ mg mg}^{-1} \text{ h}^{-1}$) $\delta^{11}\text{B}$ of the precipitated calcite gets 1.4‰ heavier for a temperature increase of 10 °C. Additionally, calcites precipitated at the same temperature (22 °C) but different growth record values that are 2.1‰ lighter for a doubling of growth rate. As discussed earlier, the fundamental assumption on which the $\delta^{11}\text{B}$ -pH proxy is based is that $\text{B}(\text{OH})_4^-$ is preferentially incorporated into calcite over the neutral $\text{B}(\text{OH})_3$. Hence, in an ideal scenario

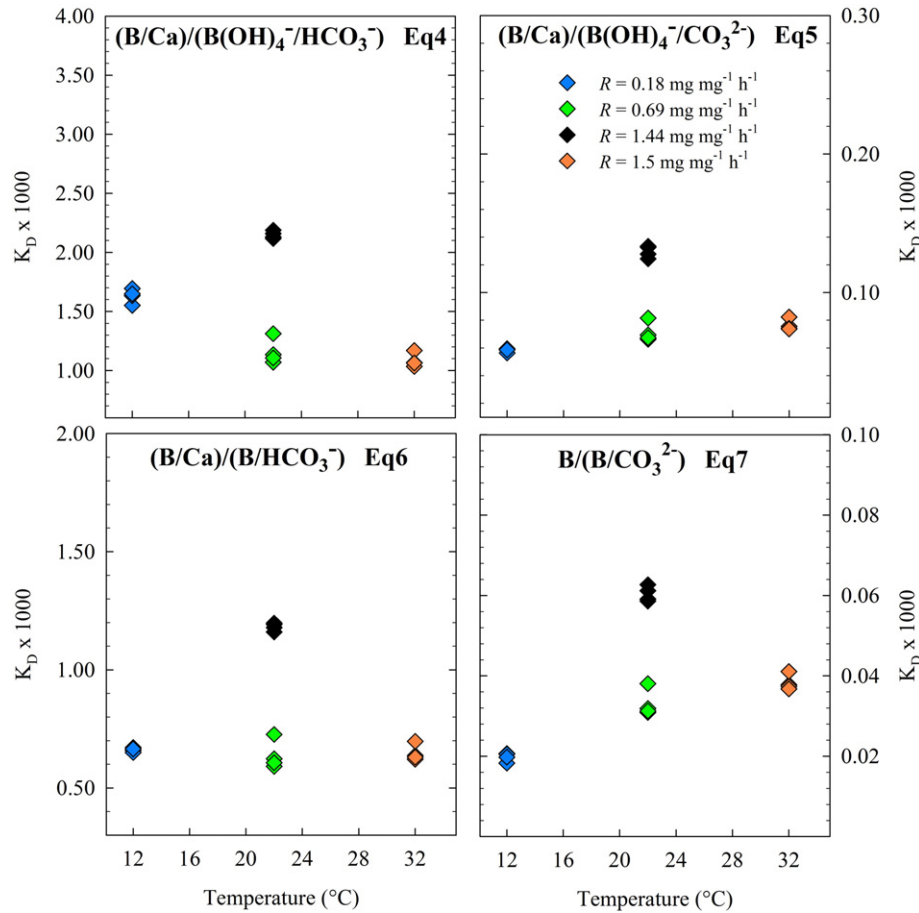


Fig. 3. K_D values calculated according to Eqs. (4) to (7). An effect of growth rate (green + black diamonds) and of temperature (orange + black diamonds) is observed. Uncertainties are given in Table 3, information on the calculation of uncertainties is given in the Appendix A. Note different y-axis scales.

the $\delta^{11}\text{B}_{\text{calcite}}$ should be identical to the $\delta^{11}\text{B}_{\text{B(OH)}_4^-}$ of the solution. Therefore, the B fractionation (ε) between $\delta^{11}\text{B}_{\text{calcite}}$ and $\delta^{11}\text{B}_{\text{B(OH)}_4^-}$ ($\varepsilon = \delta^{11}\text{B}_{\text{calcite}} - \delta^{11}\text{B}_{\text{B(OH)}_4^-}$) should be 0‰. To evaluate ε , the $\delta^{11}\text{B}_{\text{B(OH)}_4^-}$ was calculated using (Zeebe and Wolf-Gladrow, 2001):

$$\delta^{11}\text{B}_{\text{B(OH)}_4^-} = \frac{\delta^{11}\text{B} \times [\text{B}] - \varepsilon_{\text{B}} \times [\text{B(OH)}_3]}{[\text{B(OH)}_4^-] + \alpha_{\text{B}} \times [\text{B(OH)}_3]} \quad (8)$$

where $\delta^{11}\text{B}$, $[\text{B}]$, $[\text{B(OH)}_4^-]$, and $[\text{B(OH)}_3]$ refer to the growth solution (as given in Table 1). α_{B} is the fractionation factor between B(OH)_4^- and

B(OH)_3 ($\alpha_{\text{B}} = 1.0250$ Klochko et al., 2006) and $\varepsilon_{\text{B}} = (\alpha_{\text{B}} - 1) \times 1000$. A detailed discussion about α_{B} is given in Section 4.2. Calculations of the uncertainties of $\delta^{11}\text{B}_{\text{B(OH)}_4^-}$ and ε are provided in the Appendix A. In Fig. 4 ε is plotted for each run. The results show a significant effect of R on ε . Treatments performed at a constant T (22 °C) but variable R (green and black diamonds in Fig. 4) demonstrate on average a lighter ε by 1‰ if R is doubled. Treatments conducted at a constant R ($\sim 1.5 \text{ mg mg}^{-1} \text{ h}^{-1}$) but variable T (black and orange diamonds in Fig. 4) show no significant effect of T on ε within a temperature range of 10 °C.

Table 3

Boron partition coefficients calculated according to (4)–(7). Details on calculation of uncertainties are given in the Appendix A.

$K_D \times 1000$ Eq. (4)	$2\sigma \times 1000$	$K_D \times 1000$ Eq. (5)	$2\sigma \times 1000$	$K_D \times 1000$ Eq. (6)	$2\sigma \times 1000$	$K_D \times 1000$ Eq. (7)	$2\sigma \times 1000$
1.695	0.004	0.056	7E-05	0.659	8E-05	0.0183	0.0002
1.551	0.004	0.059	7E-05	0.650	8E-05	0.0207	0.0002
1.634	0.004	0.059	7E-05	0.671	7E-05	0.0205	0.0002
1.650	0.004	0.059	7E-05	0.665	8E-05	0.0198	0.0002
1.311	0.003	0.082	1E-04	0.726	5E-05	0.0381	0.0002
1.135	0.003	0.069	9E-05	0.623	5E-05	0.0319	0.0002
1.070	0.003	0.066	8E-05	0.591	5E-05	0.0309	0.0002
1.106	0.003	0.067	8E-05	0.607	5E-05	0.0313	0.0002
2.118	0.005	0.124	2E-04	1.178	5E-05	0.0586	0.0002
2.159	0.005	0.133	2E-04	1.192	5E-05	0.0627	0.0002
2.187	0.006	0.133	2E-04	1.198	5E-05	0.0612	0.0002
2.130	0.005	0.128	2E-04	1.160	5E-05	0.0591	0.0002
1.067	0.003	0.076	9E-05	0.637	5E-05	0.0378	0.0002
1.170	0.002	0.082	7E-05	0.697	6E-05	0.0411	0.0002
1.034	0.002	0.074	6E-05	0.621	6E-05	0.0374	0.0002
1.064	0.003	0.074	9E-05	0.630	5E-05	0.0368	0.0002

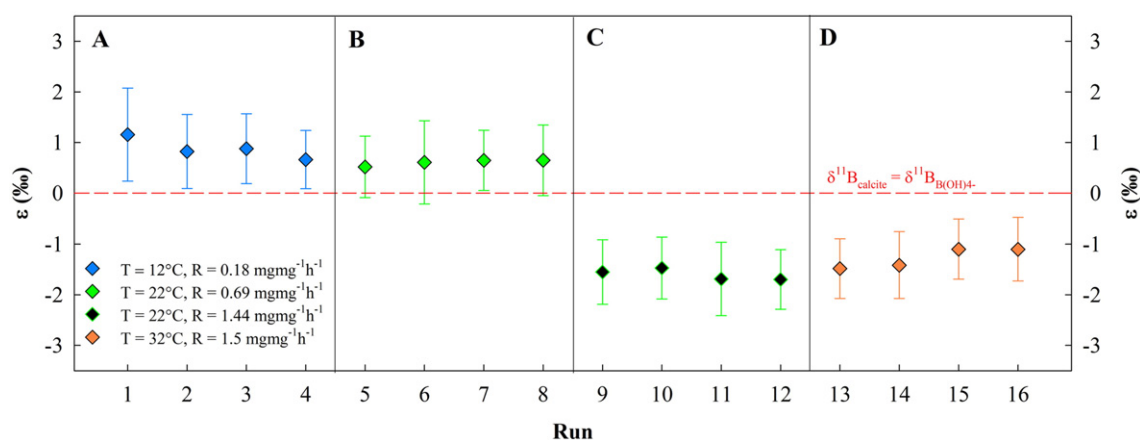


Fig. 4. Fractionation (ϵ) between calcite and B(OH)_4^- . On the zero-line $\delta^{11}\text{B}_{\text{calcite}}$ equals $\delta^{11}\text{B}_{\text{B(OH)}_4^-}$. Positive ϵ values represent a heavier $\delta^{11}\text{B}_{\text{calcite}}$ than $\delta^{11}\text{B}_{\text{B(OH)}_4^-}$, negative values a lighter $\delta^{11}\text{B}_{\text{calcite}}$ than $\delta^{11}\text{B}_{\text{B(OH)}_4^-}$. For the calculation of uncertainties on ϵ see Appendix A. Comparison of (B) and (C) show a significant growth rate effect on ϵ of $\sim 1\%$.

Due to the B dilution mean values of $[\text{B(OH)}_3]$, $[\text{B}]$, and $[\text{B(OH)}_4^-]$ (as listed in Table 1) were used for the calculation of $\delta^{11}\text{B}$ of B(OH)_4^- .

4. Discussion

4.1. Boron concentration

4.1.1. Effect of growth rate on the B incorporation into calcite

The effect of growth rate on B incorporation into calcite observed in this study is in good agreement with published work (Gabitov et al., 2014; Uchikawa et al., 2015; Mavromatis et al., 2015). Gabitov et al. (2014) determined calcite growth rate by successively spiking the growth solution with REE, which meant that the width of each spiked zone grown per given time interval was analogous to the growth rate. Gabitov et al. (2014) demonstrated that the growth rate decreased in a radially outward direction, from the inside to the outside of the crystal, with higher concentration of B observed towards the inside of the crystal. Uchikawa et al. (2015) performed seeded calcite precipitation experiments in a growth medium at constant pH by adding a Na_2CO_3 titrant through the course of the precipitation experiments, an experimental design similar to ours. A positive correlation between growth rate and the amount of B incorporated into calcite was documented by this study. Mavromatis et al. (2015) utilized a mixed-flow reactor for seeded and non-seeded calcite precipitation. For both types of experiments a positive correlation between growth rate and B co-precipitation into calcite was observed. Irrespective of the experimental approach all studies (including ours) confirm a higher B incorporation at faster calcite growth rate.

Sen et al. (1994) and Hemming et al. (1995) suggested that B undergoes a structural change from tetrahedral to trigonal coordination before its incorporation into calcite. Ruiz-Agudo et al. (2012) performed AFM measurements on the surface of a growing calcite crystal and suggested that the B coordination change from tetrahedral to trigonal could represent the rate limiting step for B incorporation. Following this suggestion a decreased B incorporation at higher growth rates is expected since less time for B re-coordination is available. However, this notion contradicts the results of Gabitov et al. (2014); Uchikawa et al. (2015); Mavromatis et al. (2015), and our study that demonstrated a higher B co-precipitation with increasing growth rate. Mavromatis et al. (2015) demonstrated that the amount of trigonal-coordinated B in calcite decreases with increasing growth rate. This validates that the reported re-coordination from tetrahedral to trigonal B on the surface of the growing calcite crystal is not essential for B incorporation.

4.1.2. Effect of temperature on the B incorporation into calcite

Our results show a definite temperature dependence of the B concentrations and subsequently K_D . However, a contradictory observation of a temperature independence of the partition coefficient within a

temperature range of 20 °C is reported in Mavromatis et al. (2015). Yet, only two of the experiments of Mavromatis et al. (2015) allow an adequately comparison to investigate a temperature effect, these are CaB-11(s) and CaB-15(s). These experiments have equal pH, $[\text{B}]$, Ω , and precipitation rates and the similar B partition coefficients suggest no temperature effect on B co-precipitation. However, no duplicates or triplicates were performed to support the data. Future work is essential to resolve this difference. Although we cannot definitely explain the observed differences, we propose a potential mechanism that explains the temperature dependence of B incorporation in Section 4.1.4.

4.1.3. Comparison between B partition coefficients

Our results for the different definitions of K_D from experiments performed at 22 and 32 °C show an identical trend when K_D is plotted as a function of temperature and growth rate. For K_D values for which B(OH)_4^- is replaced with $[\text{B}]$ in the denominator (Eqs. (4),(6),(7)) the effects of T and R are still visible because $[\text{B(OH)}_4^-]$ and $[\text{B}]$ do not change among treatments (Table 1). Following the same reasoning, it makes no difference whether B/Ca or total B in the numerator is chosen. Replacing $[\text{HCO}_3^-]$ by $[\text{CO}_3^{2-}]$ in the denominator (Eqs. (4) and (5)) results in a different pattern for the treatment performed at 12 °C if compared to treatments performed at 22 and 32 °C. This difference stems from the fact that among the treatments $[\text{CO}_3^{2-}]$ is lowest and $[\text{HCO}_3^-]$ is highest at 12 °C (Table 1).

4.1.4. The surface entrapment model

For a better understanding of B co-precipitation in calcite we distinguish between the effect of growth rate and temperature by means of the so called surface entrapment model (SEMO) which was conceived to explain trace/minor element incorporation and isotope fractionation during crystal growth (Watson and Liang, 1995; Watson, 1996, 2004). SEMO has been successfully applied to experimental data for e.g. Sr incorporation (Tang et al., 2008b) and Ca isotope fractionation (Tang et al., 2008a) in calcite. The SEMO is based on the following major assumption: (1) Within a thin surface layer of a crystal in equilibrium with an aqueous solution, the so called “surface boundary layer” (S), trace/minor elements are enriched compared to their concentration in the bulk of the crystal lattice (e.g. Hall, 1953; Tiller and Ahn, 1980) (2) The concentration of the trace/minor element in S exponentially increases towards the crystal surface following (Tiller and Ahn, 1980):

$$C_t = C_{eq} \times F^{\exp(x/l)} \quad (9)$$

where C_t is the concentration of the trace/minor elements at some distance x from the crystal surface, C_{eq} represents the equilibrium concentration with respect to C_t between the crystal lattice and the growth medium, ‘F’ is the surface entrapment factor defined as the ratio

between the trace/minor element concentration of the crystal surface and the bulk lattice concentration reflecting equilibrium condition, and ' l ' is the half-thickness of the surface layer. (3) The enrichment of a trace/minor element in the surface boundary layer relative to the bulk crystal implies that the crystal lattice structure at the near surface differs from the bulk lattice. Using *in situ* high resolution X-ray reflectivity Fenter et al. (2000) concluded that the outermost two monolayers of a calcite crystal have a different structure from the bulk crystal in terms of orientation and bond length. This structural difference is thought to allow ions to move more freely i.e. the diffusivity of ions within that region of the lattice should be greater than in the bulk crystal (Watson, 2004). This hypothesis is supported by multiple observations of enhanced near-surface ion mobility (Stipp et al., 1992; Stipp, 1998; Hoffmann and Stipp, 2001). During the growth of the crystal the fate of the trace elements in the surface layer depends on two major processes: (1) diffusivity of the trace elements between S and the newly precipitated crystal layer (C_1) and (2) the growth rate of this newly precipitated crystal layer. The outcome of these two competitive processes dictates the final enrichment or depletion of the trace/minor element in the newly forming crystal layer (C_1): If the diffusivity of the trace/minor element is faster than the growth rate of the crystal, then the trace/minor element is depleted in the newly precipitated crystal layer (C_1). On the other hand, if the growth rate of the crystal layer is faster than the diffusivity of the trace/minor element, then the trace/minor element is enriched in the newly formed layer (C_1).

Fig. 5 illustrates the B incorporation into calcite based on the SEMO concept and our data. Note, our results demonstrate that a qualitative approach of the SEMO concept is suitable to significantly broaden our understanding of the B incorporation into inorganic calcite.

4.1.4.1. Constant temperature – variable growth rates. According to the SEMO crystals grown at the same temperature show the same diffusivity for B in S. With increasing growth rate the newly forming crystal layer

(C_1) is building faster, which leaves less time for B to diffuse out of C_1 into S while C_1 successively becomes part of the bulk lattice of the crystal. Consequently, the entrapment of B in this new layer C_1 is more effective at higher growth rates. This model prediction is in good agreement with our experimental results. In experiments performed at the same temperature (22 °C) our results show on average an increase of the B concentration from 61 to 114 mg/kg and all K_D values if the growth rate increases from 0.69 to 1.44 $\text{mg mg}^{-1} \text{h}^{-1}$ (Fig. 5A + B).

4.1.4.2. Constant growth rate – variable temperatures. If two crystals grow at the same rate, the SEMO predicts that elevated temperatures lead to higher ion diffusivity within S resulting in a faster “escape” of B from the newly forming layer C_1 into the S layer. In case of crystals having the same growth rate the amount of layers added per time unit is identical i.e. results in the same thickness of C_1 . Applying this scenario to the B incorporation into calcite predicts that with increasing temperatures the diffusivity of B out of C_1 is enhanced and more B can escape from C_1 before C_1 can be completed i.e. becomes part of the bulk crystal lattice. Our results follow this prediction. Experiments performed at a constant growth rate of $\sim 1.5 \text{ mg mg}^{-1} \text{h}^{-1}$ show on average a decrease in B concentration from 114 to 56 mg/kg and in all K_D values if temperature is increased from 22 to 32 °C (Fig. 5C + D).

In summary we demonstrated that the effect of growth rate and temperature on the incorporation of B into calcite can be explained by the SEMO. Kinetic and temperature effects of Sr^{2+} into CaCO_3 have also been successfully explained by the SEMO in the study of Tang et al. (2008b). This suggests that the incorporation of two so different ions, Sr^{2+} being a divalent cation substituted for Ca^{2+} in the calcite lattice and B, incorporated at a CO_3^{2-} site or/and occupying a defect or non-lattice site, can be explained by the same processes. However, with respect to the study by Tang et al. (2008b) it is important to note that in order to obtain a good fit between the model calculations and

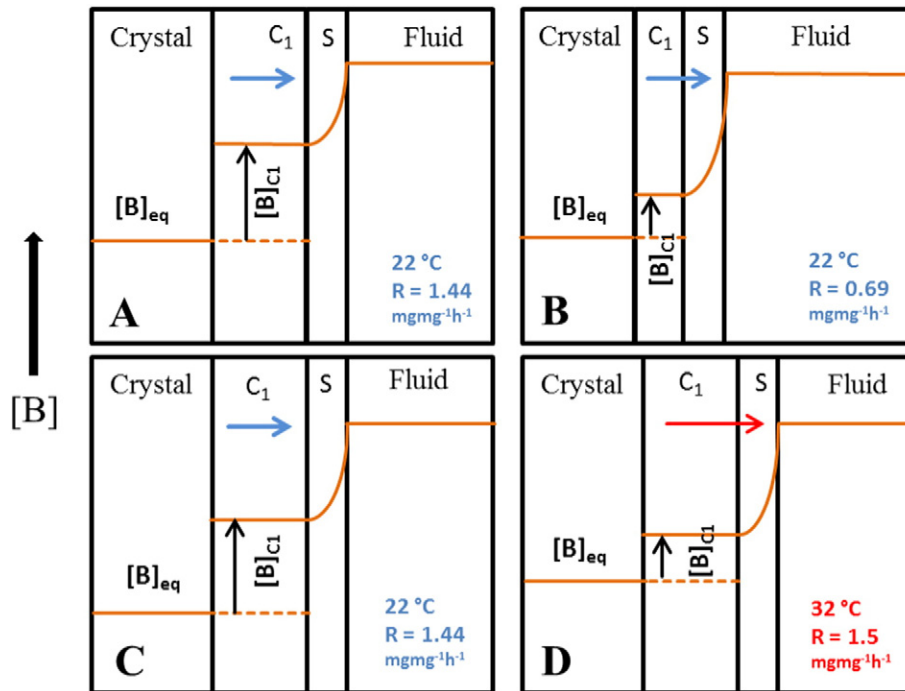


Fig. 5. The SEMO concept considering temperature and growth rate effects on boron incorporation. The orange line represents B concentration in four compartments: the crystal, the newly precipitated calcite (C_1), the surface layer (S), and the fluid; $[\text{B}]_{\text{eq}}$ is the boron concentration in equilibrium of the crystal with the solution, $[\text{B}]_{C_1}$ represents the amount of B being incorporated into C_1 . The enrichment of B in S is described by Eq. (9) (A + B) Constant temperature (22 °C) variable growth rates: At the same temperature the B diffusivity is equal in both experiments (indicated by the blue arrows). At a higher growth rate (A) the distance for B to diffuse out from C_1 into S is larger than at a lower growth rate (B). As a consequence B is more efficiently entrapped at a higher growth rate in C_1 (indicated by the black arrows). (C + D) Constant growth rate ($\sim 1.5 \text{ mg mg}^{-1} \text{h}^{-1}$) variable temperatures: At a constant growth rate the distance for B to diffuse out from C_1 into S is equal in both experiments. Boron diffusivity is higher at 32 °C (as indicated by the red arrow) leading to a more effective escape from C_1 into S. Consequently, B incorporation is reduced at higher temperature in C_1 (indicated by the black arrows). It should be noted that the difference in $[\text{B}]_{\text{eq}}$ at 22 and 32 °C is difficult to quantify since the temperature dependence of $[\text{B}]_{\text{eq}}$ is not known.

their experimental data, the value for D_s (Sr diffusion coefficient in the surface layer) had to be set 16 (!) orders of magnitude higher than reported in the literature for diffusion in the bulk crystal. A numerical simulation in which the SEMO was applied to the B incorporation into calcite can be found in Gabitov et al. (2014). These authors also concluded that the observed growth rate effect on K_D can be explained by the surface entrapment model. However, the agreement between experimental and model data is based on an optimization of the D_s value which was arbitrarily chosen. One challenge for using model calculations like SEMO is the lack of knowledge of parameters such as D_s and F required for modelling. Thus, further investigations are required to quantify these parameters and to create a solid basis for the combination of experimental work and theoretical calculations.

4.1.5. Surface kinetic model

Kinetically controlled element partitioning and isotope fractionation could also be explained by the Surface Kinetic Model (SKMO) by DePaolo (2011). SKMO considers minor/trace element partitioning and isotope fractionation as a competition between the net precipitation rate (R_p) and the bulk backward reaction (R_b) i.e. dissolution. The ratio of the net precipitation rate (R_p) and bulk backward reaction (R_b) dictates the composition of the crystal: R_p/R_b values lower than 1 represent precipitation close to equilibrium conditions whereas higher R_p/R_b feature precipitation controlled by kinetic fractionation. The SKMO can also be considered as a growth entrapment model but here growth rate competes with the rate of molecular exchange between the mineral surface and solution. SKMO has been successfully tested on a number of experimental data obtained from several studies with respect to minor/trace element partitioning (Tang et al., 2008b; Lorens, 1981; Tesoriero and Pankow, 1996) and isotope fractionation (Tang et al., 2008a). Due to the consistency between Sr co-precipitation and SKMO as well as SEMO (as shown in DePaolo, 2011; Tang et al., 2008b) and the consistency between the experimental data of Tang et al. (2008b) and ours we can assume that B co-precipitation would be consistent with SKMO, too. However, similar to using SEMO the application of SKMO is restricted to the knowledge of parameters such as R_p , R_b , and equilibrium and kinetic fractionation factors. For B these parameters are still unknown or currently under debate and a more detailed discussion of the SKMO in the framework of this study is not approached since any results would stay speculative.

4.1.6. Further consideration

We prepared our growth solutions in such a way that the effects of temperature and growth rate on B incorporation into calcite are decoupled. Due to this manipulation our system is different from most natural aqueous systems in which a change in temperature would subsequently alter the growth rate of calcite. It is important to note that in natural settings the opposing effects of temperature and growth rate on the B co-precipitation (as visible in a decoupled system from our study) may cancel each other out if their effects are of equal magnitudes.

4.2. Boron isotopes

Fig. 4 demonstrates that ϵ depends on the growth rate of calcite. Since the value of ϵ strongly depends on the choice of α_B we will shortly discuss the problems involved in the right choice of α_B before we continue our discussion on the B isotope composition as a function of the growth rate of calcite. The first theoretical estimate of α_B was 1.0194 (Kakihana et al., 1977) based on reduced partition function calculations from spectroscopic data on molecular vibrations. Subsequent studies using *ab initio* calculations and semi-empirical modeling determined higher values of α_B ($\alpha_B = 1.027 - 1.036$ Oi, 2000; $\alpha_B = 1.027$ Liu and Tossell, 2005; $\alpha_B = 1.026 - 1.028$ Rustad et al., 2010). Zeebe (2005) showed that the calculation of α_B is sensitive to the choice of the theoretical method used to calculate the forces in the molecule and the molecular vibration frequencies. Therefore, the need for an independent, experimentally determined α_B was highlighted. Klochko

et al. (2006) determined α_B experimentally from spectroscopic pH measurements from differences in the pK_B of $^{11}\text{B}(\text{OH})_3$ and $^{10}\text{B}(\text{OH})_3$ to be 1.0272 ± 0.0003 (2σ) for seawater ($I = 0.74$) at 25 °C and 1.025 ± 0.0005 (2σ) for KCl solutions ($I = 0.62$). The value for α_B determined by Klochko et al. (2006) represents the most widely used one in the field of paleo pH-reconstructions. More recently, Nir et al. (2015) determined α_B to be 1.026 ± 0.001 within errors in the same range as the value determined by Klochko et al. (2006). The major difference between these two studies is that Nir et al. (2015) claim that α_B is independent of the solution matrix (e.g. I) whereas Klochko et al. (2006) reported a significant dependence of α_B on the solution matrix. In the following we base our B isotope data interpretation on α_B determined by Klochko et al. (2006) because (1) the uncertainty of α_B given by Klochko et al. (2006) is smaller which has consequences for the uncertainty estimations of $\delta^{11}\text{B}_{\text{B}(\text{OH})_4^-}$ and ϵ in our study (2) we want to take a potential effect of I on α_B into account. The ϵ values presented in Fig. 4 are based on $\alpha_B = 1.025$ ($I = 0.62$) since this value corresponds best to the ionic strength of our solutions ($I = 0.61$) rather than α_B of 1.0272 which is determined for a seawater matrix. An effect of temperature on α_B is likely, however, the exact magnitude of the temperature influence has not been determined so far. Several studies used theoretical approaches to assess this issue and Zeebe (2005) pointed out that the magnitude of the temperature influence depends on the frequencies used in the calculations. Klochko et al. (2006) determined experimentally α_B to be temperature independent within a range of 15 °C. They report, however, a large uncertainty of α_B at 40 °C which could easily mask a potential temperature effect on α_B . At this stage we therefore consider the influence of temperature on α_B as being smaller than the analytical uncertainty.

Fig. 4A shows that ϵ values determined for the experiment with the slowest calcite growth rate are slightly above 0. Based on the general assumption that only $\text{B}(\text{OH})_4^-$ is incorporated into calcite, we would not expect values of ϵ to be >0 . However, if α_B is decreased by only 0.5% (i.e. to 1.02455), ϵ would already become 0 within its uncertainty for the experiment with the slowest growth rate (Fig. 4A). As the determination of the exact α_B value still represents an ongoing task and our observed growth rate dependence of the B isotope fractionation does not depend on the absolute value of ϵ but rather on its relative change with growth rate, the small offset of ϵ from the zero value (Fig. 4A) can be regarded as irrelevant for the further discussion.

4.2.1. Effect of growth rate on the B isotope fractionation

Zeebe et al. (2001) calculated the time required for establishing the isotopic equilibrium between $\text{B}(\text{OH})_3$ and $\text{B}(\text{OH})_4^-$ in seawater to be $\sim 125 \mu\text{s}$. The authors concluded that kinetic fractionation during B co-precipitation into calcite is unlikely since the time required for establishing B isotopic equilibrium is very short compared to the time scales of calcite growth. However, Zeebe et al. (2001) refer to a B isotopic equilibrium between calcite and solution without taking into account any kinetic processes within the surface layer of a growing calcite crystal. Several processes at a growing calcite surface can potentially affect the incorporation of B isotopes independent of how fast equilibrium between $\text{B}(\text{OH})_3$ and $\text{B}(\text{OH})_4^-$ in solution is established. For example, Gussone et al. (2003) state that: "kinetic isotope fractionation occurs at any boundary layer from one phase to another because lighter isotopes always tend to diffuse faster than heavier isotopes". In addition, it has been shown that calcite surface reactivity is directly related to crystal topography (Wolthers et al., 2013). Given the fact that crystal topography is influenced by growth rate, it is questionable whether B isotope fractionation during calcite precipitation can be explained without taking these processes into account. The recently observed growth rate dependence on B re-coordination (Mavromatis et al. (2015)) before its incorporation into inorganically precipitated calcite illustrates that the processes occurring on a calcite surface with relation to B fractionation are far from being understood. Detailed modelling studies characterizing the processes at the growing calcite surface are needed to understand this observation and possible consequences for $\delta^{11}\text{B}$ signatures.

4.2.2. Other studies on B isotopes

Sanyal et al. (2000) performed inorganic calcite precipitation experiments at different growth rates realized by varying the pH of the growth solutions. The authors indicate that they do not observe a growth rate effect on B isotopic composition of calcite. Unfortunately, an evaluation of their $\delta^{11}\text{B}_{\text{B(OH)}_4^-}$ and $\delta^{11}\text{B}_{\text{calcite}}$ data is difficult since important information for calculating $\delta^{11}\text{B}_{\text{B(OH)}_4^-}$ are not provided in the paper. For example, it is not clear which $\text{p}K_{\text{B}}$ value was used to calculate $\delta^{11}\text{B}_{\text{B(OH)}_4^-}$. Given that $\text{p}K_{\text{B}}$ is a function of temperature the missing temperature information (temperature is vaguely given as “ambient laboratory temperature”) and the stated temperature variability of several °C during the course of their experiments makes it impossible to re-calculate $\delta^{11}\text{B}_{\text{B(OH)}_4^-}$. Furthermore, an $\alpha_{\text{B}} = 1.0194$ (Kakihana et al., 1977) was used for the determination of $\delta^{11}\text{B}_{\text{B(OH)}_4^-}$. For comparison with our data a re-calculation of $\delta^{11}\text{B}_{\text{B(OH)}_4^-}$ is necessary using $\alpha_{\text{B}} = 1.0272$. However, this can only be done adequately if $\text{p}K_{\text{B}}$ for the specific experimental conditions is known.

Gabitov et al.'s (2014) investigation of a potential growth rate effect on B isotope fractionation in calcite was restricted by a large analytical uncertainty of 4‰ (2 σ). Thus, Gabitov et al. (2014) could only conclude that if there is an effect of growth rate on $\delta^{11}\text{B}$ it must be smaller than 4‰. The precision of our $\delta^{11}\text{B}$ data is high enough to show that within our experimental conditions a doubling of the growth rate causes a 1‰ shift towards lighter $\delta^{11}\text{B}_{\text{calcite}}$.

5. Conclusion and implications

Our inorganic calcite precipitation experiments confirm the positive growth rate effect on B co-precipitation recently shown by several other studies (Gabitov et al., 2014; Uchikawa et al., 2015; Mavromatis et al., 2015). In contrast to the results of Mavromatis et al. (2015) our data show a clear negative temperature effect on B incorporation. Furthermore, we could demonstrate that the boron isotope signature of calcite gets lighter with increasing growth rate. Boron partitioning into calcite as a function of growth rate and temperature can be explained by the so called surface entrapment model.

It is difficult to evaluate whether these findings, determined for a purely inorganic system, will have direct implications in the interpretation of B data determined in the context of paleo-reconstructions. In the study of Gabitov et al. (2014) the authors state that “A growth rate effect on boron partitioning into carbonate minerals could explain the variety of relationships between B/Ca ratios and carbonate system parameters determined for foraminifera and other types of calcite.” Uchikawa et al. (2015) on the other hand pointed out that the uncertainties in the determination of precipitation rates of biogenically formed calcite make it difficult to translate relationships determined from an inorganic system to a biogenic system. We concur with Uchikawa et al. (2015) that it is currently impossible to determine a meaningful and reliable growth rate for calcifying organisms that could be compared to an inorganic system.

The strong effect of temperature on the B incorporation observed in this study is not seen for foraminifers from culture studies (Allen et al., 2011, 2012; Babila et al., 2014). However, a direct comparison of an inorganic and a biogenic system is not possible, because it is currently unknown how calcification rate and other important physiological processes of the foraminifer or their symbionts, that could affect the B incorporation, are affected by temperature. Therefore, it will be a major challenge for future studies to deconvolve the impact of temperature and calcification rate on boron partitioning and fractionation in biogenic systems to develop a mechanistic understanding of the B proxy.

Acknowledgments

We thank Sarah Moser and Kerstin Oetjen for assistance during the experiments. For analysis of DIC and elemental measurements we thank Laura Wischniewski, Jana Hölscher and Ilsetraut Stöltzing. We thank Dieter Wolf-Gladrow for his support in calculating error propagations using Matlab. This project was financially supported by a DFG grant to JB (BI 432/7-1) and in part by The European Research Council (ERC grant 2010-NEWLOG ADG-267931 HE).

Appendix A. Calculation of uncertainties

A.1. Boron partition coefficient (K_D)

The uncertainties of K_D values are given by:

$$2\sigma_{K_D}(\text{Eq 4}) = \sqrt{\left(\frac{\partial K_D}{\partial [\text{B}]} \sigma_{[\text{B}]}\right)_{\text{calcite}}^2 + \left(\frac{\partial K_D}{\partial [\text{B(OH)}_4^-]} \sigma_{[\text{B(OH)}_4^-]}\right)_{\text{fluid}}^2 + \left(\frac{\partial K_D}{\partial [\text{HCO}_3^-]} \sigma_{[\text{HCO}_3^-]}\right)_{\text{fluid}}^2} \times 2 \quad (\text{A1})$$

$$2\sigma_{K_D}(\text{Eq 5}) = \sqrt{\left(\frac{\partial K_D}{\partial [\text{B}]} \sigma_{[\text{B}]}\right)_{\text{calcite}}^2 + \left(\frac{\partial K_D}{\partial [\text{B(OH)}_4^-]} \sigma_{[\text{B(OH)}_4^-]}\right)_{\text{fluid}}^2 + \left(\frac{\partial K_D}{\partial [\text{CO}_3^{2-}]} \sigma_{[\text{CO}_3^{2-}]}\right)_{\text{fluid}}^2} \times 2 \quad (\text{A2})$$

$$2\sigma_{K_D}(\text{Eq 6}) = \sqrt{\left(\frac{\partial K_D}{\partial [\text{B}]} \sigma_{[\text{B}]}\right)_{\text{calcite}}^2 + \left(\frac{\partial K_D}{\partial [\text{HCO}_3^-]} \sigma_{[\text{HCO}_3^-]}\right)_{\text{fluid}}^2} \times 2 \quad (\text{A3})$$

$$2\sigma_{K_D}(\text{Eq 7}) = \sqrt{\left(\frac{\partial K_D}{\partial [B]} \sigma_{[B]} \right)_{\text{calcite}}^2 + \left(\frac{\partial K_D}{\partial [CO_3^{2-}]} \sigma_{[CO_3^{2-}]} \right)_{\text{fluid}}^2} \times 2 \quad (\text{A4})$$

The concentration of B_{calcite} is given in Table 2, concentrations of $B(OH)_4^-$, and HCO_3^- are listed in Table 1. The uncertainty of $[B]_{\text{fluid}}$ as estimated by multiple measurements of the reference material is $\pm 4\%$. The uncertainties of $[B(OH)_4^-]_{\text{fluid}}$, $[HCO_3^-]_{\text{fluid}}$, and $[CO_3^{2-}]_{\text{fluid}}$ were calculated according to:

$$\sigma_{[B(OH)_4^-]} = \sqrt{\left(\frac{\partial [B(OH)_4^-]}{\partial [B]} \sigma_{[B]} \right)^2 + \left(\frac{\partial [B(OH)_4^-]}{\partial [H^+]} \sigma_{[H^+]} \right)^2} \quad (\text{A5})$$

$$\sigma_{[HCO_3^-]} = \sqrt{\left(\frac{\partial [HCO_3^-]}{\partial [DIC]} \sigma_{[DIC]} \right)^2 + \left(\frac{\partial [HCO_3^-]}{\partial [H^+]} \sigma_{[H^+]} \right)^2 + \left(\frac{\partial [HCO_3^-]}{\partial K_1} \sigma_{K_1} \right)^2 + \left(\frac{\partial [HCO_3^-]}{\partial K_2} \sigma_{K_2} \right)^2} \quad (\text{A6})$$

$$\sigma_{[CO_3^{2-}]} = \sqrt{\left(\frac{\partial [CO_3^{2-}]}{\partial [DIC]} \sigma_{[DIC]} \right)^2 + \left(\frac{\partial [CO_3^{2-}]}{\partial [H^+]} \sigma_{[H^+]} \right)^2 + \left(\frac{\partial [CO_3^{2-}]}{\partial K_1} \sigma_{K_1} \right)^2 + \left(\frac{\partial [CO_3^{2-}]}{\partial K_2} \sigma_{K_2} \right)^2} \quad (\text{A7})$$

The uncertainty of H^+ represents the SD for each run. The error of DIC is estimated by the reproducibility of measurements and is $\pm 10 \mu\text{mol/l}$. For the dissociation constant of B (K_B) no error estimation is reported in the literature (Owen and King, 1943). For the dissociation constants of C (K_1 , K_2) the uncertainties are 0.002 and 0.003, respectively (Plummer and Busenberg, 1982).

A.2. Epsilon

The uncertainty of ε is given by:

$$2\sigma_\varepsilon = \sqrt{\left(\frac{\partial \varepsilon}{\partial \delta^{11}B_{\text{calcite}}} \sigma_{\delta^{11}B_{\text{calcite}}} \right)^2 + \left(\frac{\partial \varepsilon}{\partial \delta^{11}B(OH)_4^-} \sigma_{\delta^{11}B(OH)_4^-} \right)^2} \times 2 \quad (\text{A8})$$

The $\delta^{11}B_{\text{calcite}}$ and $\delta^{11}B_{B(OH)_4^-}$ are given in Table 2. The uncertainty of $\delta^{11}B_{\text{calcite}}$ represents the analytical error (Table 2). The uncertainty of $\delta^{11}B_{B(OH)_4^-}$ was calculated as follows:

$$\sigma_{\delta^{11}B(OH)_4^-} = \sqrt{\left(\frac{\partial \delta^{11}B_{B(OH)_4^-}}{\partial [B]} \sigma_{[B]} \right)^2 + \left(\frac{\partial \delta^{11}B_{B(OH)_4^-}}{\partial \delta^{11}B_{\text{gs}}} \sigma_{\delta^{11}B_{\text{gs}}} \right)^2 + \left(\frac{\partial \delta^{11}B_{B(OH)_4^-}}{\partial \alpha_B} \sigma_{\alpha_B} \right)^2 + \left(\frac{\partial \delta^{11}B_{B(OH)_4^-}}{\partial \varepsilon_B} \sigma_{\varepsilon_B} \right)^2 + 2 \left(\frac{\partial \delta^{11}B_{B(OH)_4^-}}{\partial [B(OH)_4^-]} \sigma_{[B(OH)_4^-]} \right)^2} \quad (\text{A9})$$

Where $\delta^{11}B_{\text{gs}}$ refers to the growth solution listed in Table 1 including its uncertainties. The B fractionation factor $\alpha_B = 1.025$ and $\sigma_{\alpha_B} = 0.00025$ (Klochko et al., 2006), $\varepsilon_B = (\alpha - 1) \times 1000$, $\sigma_{\varepsilon_B} = 0.25$.

References

- Allen, K.A., Hönisch, B., 2012. The planktonic foraminifer B/Ca proxy for seawater carbonate chemistry: a critical evaluation. *Earth Planet. Sci. Lett.* 345–348, 203–211.
- Allen, K.A., Hönisch, B., Eggins, S.M., Rosenthal, Y., 2012. Environmental controls on B/Ca in calcite tests of the tropical planktic foraminifer species *Globigerinoides ruber* and *Globigerinoides sacculifer*. *Earth Planet. Sci. Lett.* 351–352, 270–280.
- Allen, K.A., Hönisch, B., Eggins, S.M., Yu, J., Spero, H.J., Elderfield, H., 2011. Controls on boron incorporation in cultured tests of the planktic foraminifer *Orbulina universa*. *Earth Planet. Sci. Lett.* 309, 291–301.
- Babila, T.L., Rosenthal, Y., Conte, M.H., 2014. Evaluation of the biogeochemical controls on B/Ca of *Globigerinoides ruber* white from the Oceanic Flux Program, Bermuda. *Earth Planet. Sci. Lett.* 404, 67–76.
- Bartoli, G., Hönisch, B., Zeebe, R.E., 2011. Atmospheric CO_2 decline during the Pliocene intensification of Northern Hemisphere glaciations. *Paleoceanography* 26, PA4213.
- Boyle, E.A., 1988. Cadmium: chemical tracer of deepwater paleoceanography. *Paleoceanography* 3, 471–489.
- Brown, R.E., Anderson, L.D., Thomas, E., Zachos, J.C., 2011. A core-top calibration of B/Ca in the benthic foraminifers *Nuttallides umbonifera* and *Oridorsalis umbonatus*: a proxy for Cenozoic bottom water carbonate saturation. *Earth Planet. Sci. Lett.* 310, 360–368.
- Catanzaro, E.J., Champion, C.E., Garner, E.L., Marinenko, G., Sappenfield, K.M., Shields, W.R., 1970. Boric acid, isotopic, and assay standard reference materials. *Nat. Bur. Stand. (U.S.) Spec. Publ.* 260–17, p. 70.
- DePaolo, D.J., 2011. Surface kinetic model for isotopic and trace element fractionation during precipitation of calcite from aqueous solutions. *Geochim. Cosmochim. Acta* 75, 1039–1056.
- DOE, 1994. Handbook of methods for the analysis of the various parameters of the carbon dioxide system in sea water; version 2. In: Dickson, A.G., Goyet, C. (Eds.), ORNL/CDIAC-74.
- Fenter, P., Geissbühler, P., DiMasi, E., Srajer, G., Sorensen, L.B., Sturchio, N.C., 2000. Surface speciation of calcite observed in situ by high-resolution X-ray reflectivity. *Geochim. Cosmochim. Acta* 64, 1221–1228.
- Foster, G., 2008. Seawater pH, pCO_2 , and $[CO_3^{2-}]$ variations in the Caribbean Sea over the last 130 kyr: A boron isotope and B/Ca study of planktic foraminifera. *Earth Planet. Sci. Lett.* 271, 254–266.
- Foster, G.L., Lear, C.H., Rae, J.W.B., 2012. The evolution of pCO_2 , ice volume and climate during the middle Miocene. *Earth Planet. Sci. Lett.* 341–344, 243–254.
- Foster, G.L., Pogge von Strandmann, P.A.E., Rae, J.W.B., 2010. Boron and magnesium isotopic composition of seawater. *Geochim. Geophys. Geosyst.* 11, Q08015.
- Gabitov, R.I., Watson, E.B., 2006. Partitioning of strontium between calcite and fluid. *Geochim. Geophys. Geosyst.* 7, 1–12.
- Gabitov, R.I., Rollion-Bard, C., Tripathi, A., Sadekov, A., 2014. In situ study of boron partitioning between calcite and fluid at different crystal growth rates. *Geochim. Cosmochim. Acta* 137, 81–92.
- Gaillardet, J., Lemarchand, D., Gopel, C., Manhès, G., 2001. Evaporation and sublimation of boric acid: application for boron purification from organic rich solutions. *Geostand. Newslett.* 25, 67–75.
- Gussone, N., Böhm, F., Eisenhauer, A., Dietzel, M., Heuser, A., Teichert, B.M.A., Reitner, J., Wörheide, G., Dullo, W.-C., 2005. Calcium isotope fractionation in calcite and aragonite. *Geochim. Cosmochim. Acta* 69, 4485–4494.
- Gussone, N., Eisenhauer, A., Heuser, A., Dietzel, M., Bock, B., Böhm, F., Spero, H.J., Lea, D.W., Bijma, J., Nägler, T.F., 2003. Model for kinetic effects on calcium isotope fractionation ($\delta^{44}Ca$) in inorganic aragonite and cultured planktonic foraminifera. *Geochim. Cosmochim. Acta* 67, 1375–1382.

- Gustafsson, J.P., 2008. Visual MINTeq Version 3.0.
- Hall, R.N., 1953. Segregation of impurities during the growth of germanium and silicon. *J. Phys. Chem.* 57, 836–839.
- Hemming, N.G., Hanson, G.N., 1992. Boron isotopic composition and concentration in modern marine carbonates. *Geochim. Cosmochim. Acta* 56, 537–543.
- Hemming, N.G., Reeder, R.J., Hanson, G.N., 1995. Mineral-fluid partitioning and isotopic fractionation of boron in synthetic calcium carbonate. *Geochim. Cosmochim. Acta* 59, 371–379.
- Hoffmann, U., Stipp, S.L.S., 2001. The behavior of Ni²⁺ on calcite surfaces. *Geochim. Cosmochim. Acta* 65, 4131–4139.
- Hönisch, B., Hemming, N.G., 2005. Surface ocean response to variations in pCO₂ through two full glacial cycles. *Earth Planet. Sci. Lett.* 236, 305–314.
- Hönisch, B., Bijma, J., Russel, A.D., Spero, H.J., Palmer, M.R., Zeebe, R.E., Eisenhauer, A., 2003. The influence of symbiotic photosynthesis on the boron isotopic composition of foraminifera shells. *Mar. Micropaleontol.* 49, 87–96.
- Hönisch, B., Hemming, N.G., Grotto, A.G., Amat, A., Hanson, G.N., Bijma, J., 2004. Assessing scleractinian corals as recorders for paleo-pH: empirical calibration and vital effects. *Geochim. Cosmochim. Acta* 68, 3675–3685.
- Kaczmarek, K., Langer, G., Nehrke, G., Horn, I., Misra, S., Janse, M., Bijma, J., 2015. Boron incorporation in the foraminifer *Amphistegina lessonii* under a decoupled carbonate chemistry. *Biogeosciences* 12, 1753–1763 (b).
- Kakihana, H., Kotaka, M., Satoh, S., Nomura, M., Okamoto, M., 1977. Fundamental studies on the ion-exchange separation of boron isotopes. *Bull. Chem. Soc. Jpn.* 50, 158–163.
- Klochko, K., Kaufman, A.J., Yao, W., Byrne, R.H., Tossell, J.A., 2006. Experimental measurement of boron isotope fractionation in seawater. *Earth Planet. Sci. Lett.* 248, 276–285.
- Liu, Y., Tossell, J.A., 2005. Ab initio molecular orbital calculations for boron isotope fractionation on boric acids and borates. *Geochim. Cosmochim. Acta* 69, 3995–4006.
- Lorens, R.B., 1981. Sr, Cd, Mn and Co distribution coefficients in calcite as a function of calcite precipitation rate. *Geochim. Cosmochim. Acta* 45, 553–561.
- Mavromatis, V., Montouillout, V., Noireaux, J., Gaillardet, J., Schott, J., 2015. Characterization of boron incorporation and speciation in calcite and aragonite from coprecipitation experiments under controlled pH, temperature and precipitation rate. *Geochim. Cosmochim. Acta* 150, 299–313.
- McIntire, W.L., 1963. Trace element partition coefficient — a review of theory and applications to geology. *Geochim. Cosmochim. Acta* 27, 1209–1264.
- Misra, S., Greaves, M., Owen, R., Kerr, J., Elmore, A.C., Elderfield, H., 2014b. Determination of B/Ca of natural carbonates by HR-ICP-MS. *Geochim. Geophys. Geosyst.* 15.
- Misra, S., Owen, R., Kerr, J., Greaves, M., Elderfield, H., 2014a. Determination of $\delta^{11}\text{B}$ by HR-ICP-MS from mass limited samples: application to natural carbonates and water samples. *Geochim. Cosmochim. Acta* 140, 531–552.
- Nehrke, G., Reichert, G.J., Van Cappellen, P., Meile, C., Bijma, J., 2007. Dependence of calcite growth rate and Sr partitioning on solution stoichiometry: non-Kossel crystal growth. *Geochim. Cosmochim. Acta* 71, 2240–2249.
- Nir, O., Vengosh, A., Harkness, J.S., Dwyer, G.S., Lahav, O., 2015. Direct measurement of the boron isotope fractionation factor: Reducing the uncertainty in reconstructing ocean paleo-pH. *Earth Planet. Sci. Lett.* 414, 1–5.
- Oi, T., 2000. Calculations of reduced partition function ratios of monomeric and dimeric boric acids and borates by the ab initio molecular orbital theory. *J. Nucl. Sci. Technol.* 37, 166–172.
- Owen, B.B., King, E.J., 1943. The effect of sodium chloride upon the ionization of boric acid at various temperatures. *J. Am. Chem. Soc.* 65, 1612–1620.
- Plummer, L.N., Busenberg, E., 1982. The solubilities of calcite, aragonite and vaterite in CO₂-H₂O solutions between 0 and 90 °C, and an evaluation of the aqueous model for the system CaCO₃-CO₂-H₂O. *Geochim. Cosmochim. Acta* 46, 1011–1040.
- Rae, J.W.B., Foster, G., Schmidt, D.N., Elliott, T., 2011. Boron isotopes and B/Ca in benthic foraminifera: proxies for the deep ocean carbonate system. *Earth Planet. Sci. Lett.* 302, 403–413.
- Reynaud, S., Hemming, N.G., Jullet-Leclerc, A., Gattuso, J., 2004. Effect of pCO₂ and temperature on the boron isotopic composition of the zooxanthellate coral *Acropora sp.* *Coral Reefs* 23, 539–546.
- Rimstidt, J.D., Balog, A., Webb, J., 1998. Distribution of trace elements between carbonate minerals and aqueous solutions. *Geochim. Cosmochim. Acta* 62, 1851–1863.
- Ruiz-Agudo, E., Putnis, C.V., Kowacz, M., Ortega-Huertas, M., Putnis, A., 2012. Boron incorporation into calcite during growth: Implications for the use of boron in carbonates as a pH proxy. *Earth Planet. Sci. Lett.* 345, 9–17.
- Rustad, J.R., Bylaska, E.J., Jackson, V.E., Dixon, D.A., 2010. Calculation of boron-isotope fractionation between B(OH)₃(aq) and B(OH)₄⁻(aq). *Geochim. Cosmochim. Acta* 74, 2843–2850.
- Sanyal, A., Bijma, J., 1999. A comparative study of the northwest Africa and eastern equatorial Pacific upwelling zones as sources of CO₂ during glacial periods based on boron isotope paleo-pH estimation. *Paleoceanography* 14, 753–759.
- Sanyal, A., Bijma, J., Spero, H., Lea, D.W., 2001. Empirical relationship between pH and the boron isotopic composition of *Globigerinoides sacculifer*: implications for the boron isotope paleo-pH proxy. *Paleoceanography* 16, 55–59.
- Sanyal, A., Hemming, N.G., Broecker, W.S., David, W.L., Spero, H.J., Hanson, G.N., 1996. Oceanic pH control on the boron isotopic composition of foraminifera: evidence from culture experiments. *Paleoceanography* 11, 513–517.
- Sanyal, A., Nugent, M., Reeder, R.J., Bijma, J., 2000. Seawater pH control on the boron isotopic composition of calcite: evidence from inorganic calcite precipitation experiments. *Geochim. Cosmochim. Acta* 64, 1551–1555.
- Sen, S., Stebbins, J.F., Hemming, N.G., Ghosh, B., 1994. Coordination environments of B impurities in calcite and aragonite polymorphs: A ¹¹B MAS NMR study. *Am. Mineral.* 79, 819–825.
- Stipp, S.L.S., 1998. Surface analytical techniques applied to calcite: evidence of solid-state diffusion and implications for isotope methods. *Palaeogeogr. Palaeoclimatol. Palaeoecol.* 140, 441–457.
- Stipp, S.L., Hochella Jr., M.F., Parks, G.A., Leckie, J.O., 1992. Cd²⁺ uptake by calcite, solid-state diffusion, and the formation of solid-solution: interface processes observed with near-surface sensitive techniques (XPS, LEED, and AES). *Geochim. Cosmochim. Acta* 56, 1941–1954.
- Su, C., Suarez, D.L., 1995. Coordination of adsorbed boron: a FTIR spectroscopic study. *Environ. Sci. Technol.* 29, 302–311.
- Tang, J., Dietzel, M., Böhm, F., Köhler, S.J., Eisenhauer, A., 2008a. Sr²⁺/Ca²⁺ and 44Ca/40Ca fractionation during inorganic calcite formation: II. Ca isotopes. *Geochim. Cosmochim. Acta* 72, 3733–3745.
- Tang, J., Köhler, S.J., Dietzel, M., 2008b. Sr²⁺/Ca²⁺ and 44Ca/40Ca fractionation during inorganic calcite formation: I. Sr incorporation. *Geochim. Cosmochim. Acta* 72, 3718–3732.
- Tesoriero, A.J., Pankow, J.F., 1996. Solid solution partitioning of Sr²⁺, Ba²⁺, and Cd²⁺ to calcite. *Geochim. Cosmochim. Acta* 60, 1053–1063.
- Tiller, W.A., Ahn, K.-S., 1980. Interface field effects on solute redistribution during crystallization. *J. Cryst. Growth* 49, 483–501.
- Uchikawa, J., Penman, D.E., Zachos, J.C., Zeebe, R.E., 2015. Experimental evidence for kinetic effects on B/Ca in synthetic calcite: Implications for potential B(OH)₄⁻ and B(OH)₃ incorporation. *Geochim. Cosmochim. Acta* 150, 171–191.
- Urey, H.C., 1947. The thermodynamic properties of isotopic substances. *J. Chem. Soc.* 562–581 (Resumed).
- Vogl, J., Rosner, M., 2012. Production and certification of a unique set of isotope and delta reference materials for boron isotope determination in geochemical, environmental and industrial materials. *Geostand. Geoanalytical Res.* 36, 161–175.
- Wang, B.-S., You, C.-F., Huang, K.-F., Wu, S.-F., Aggarwal, S.K., Chung, C.-H., Lin, P.-Y., 2010. Direct separation of boron from Na- and Ca-rich matrices by sublimation for stable isotope measurement by MC-ICP-MS. *Talanta* 82, 1378–1384.
- Watson, E.B., 1996. Surface enrichment and trace-element uptake during crystal growth. *Geochim. Cosmochim. Acta* 60, 5013–5020.
- Watson, E.B., 2004. A conceptual model for near-surface kinetic controls on the trace-element and stable isotope composition of abiogenic calcite crystals. *Geochim. Cosmochim. Acta* 68, 1473–1488.
- Watson, E.B., Liang, Y., 1995. A simple model for sector zoning in slowly grown crystals: Implications for growth rate and lattice diffusion, with emphasis on accessory minerals in crustal rocks. *Am. Mineral.* 80, 1179–1187.
- Wefer, G., Berger, W.H., Bijma, J., Fisher, G., 1999. Clues to ocean history: a brief overview of proxies. In: Fischer, G., Wefer, G. (Eds.), *Use of Proxies in Paleoceanography: Examples from the South Atlantic*. Springer, Berlin, Heidelberg, pp. 1–68.
- Wolthers, M., Di Tommaso, D., Du, Z., de Leeuw, N.H., 2013. Variations in calcite growth kinetics with surface topography: molecular dynamics simulations and process-based growth kinetics modelling. *CrystEngComm* 15, 5506–5514.
- Wolthers, M., Nehrke, G., Gustafsson, J.P., Van Cappellen, P., 2012. Calcite growth kinetics: modeling the effect of solution stoichiometry. *Geochim. Cosmochim. Acta* 77, 121–134.
- Yu, J., Elderfield, H., 2007. Benthic foraminiferal B/Ca ratios reflect deep water carbonate saturation state. *Earth Planet. Sci. Lett.* 258, 73–86.
- Yu, J., Elderfield, H., Hönisch, B., 2007. B/Ca in planktonic foraminifera as a proxy for surface seawater pH. *Paleoceanography* 22, PA2202.
- Zeebe, R.E., 2005. Stable boron isotope fractionation between dissolved B(OH)₃ and B(OH)₄⁻. *Geochim. Cosmochim. Acta* 69, 2753–2766.
- Zeebe, R.E., Wolf-Gladrow, D.A., 2001. CO₂ in seawater: equilibrium, kinetics, isotopes. Elsevier Science B.V., Amsterdam.
- Zeebe, R.E., Sanyal, A., Ortiz, J.D., Wolf-Gladrow, D.A., 2001. A theoretical study of the kinetics of the boric acid–borate equilibrium in seawater. *Mar. Chem.* 73, 113–124.